

Application of Iterative Fourier Method in Cylindrical Phaseless Antenna Measurement Technique

Jan PUSKELY

Dept. of Radio Electronics, Brno University of Technology, Purkyňova 118, 612 00 Brno, Czech Republic

puskely@feec.vutbr.cz

Abstract. *The Fourier iterative algorithm (FIA) is a well-known planar phase retrieval method. The algorithm uses conventional amplitude measurements on two surfaces placed in different distances from the measured antenna. In this paper FIA will be applied in cylindrical geometry. In this case near-field transformations use high order Hankel functions which are known to become singular in case of measurements close to AUT. In this paper we will analyze properties of Hankel function used for forward and backward transformation in FIA to make recommendations for cylindrical near-field measurement setup. We supplement FIA representing local approach with global optimization to make cylindrical phase retrieval method more robust. The proposed technique is applied for radiation pattern reconstructions of a dish antenna and a horn antenna.*

Keywords

Cylindrical near-field scanning, phaseless measurement, Fourier iterative algorithm, Hankel functions.

1. Introduction

Conventional near-field (NF) methods usually involve measurements of electric field amplitude and phase. However, phaseless methods have recently become of increasing interest to carry out antenna measurements for applications in sub-millimeter and terahertz bands where the existing phase measurement setups have their limitations [1]. Moreover, the accurate phase measurement requires sophisticated and expensive equipments [2] in comparison with phaseless methods performed by low-cost measurement setups [3].

Many different approaches have been studied in literature to solve the phase-retrieval problem [4]-[7]. One of the most significant methods has been originally formulated in the optical region and is based on Fourier iterative algorithms (FIA) [8], with the measured amplitude-only data acting as constraints. A group of the above algorithms, named also the plane-to-plane (PTP) technique, is specifically formulated for planar near-field measurements [8], [9]. They assume two sets of independent amplitude-only measurements over two distinct parallel planes and employ

the fast Fourier transform (FFT) to iteratively propagate the aperture field forward and backward between these two planes, until the prescribed tolerance is reached. These techniques belong among the local approaches and require an initial guess. It is usually determined from known AUT characteristics, rough phase measurement or by using global optimization techniques [10]-[12].

The majority of experience with FIA has been obtained for a planar surface. Although a cylindrical surface has not been used as widely, it has been demonstrated to be experimentally and computationally practicable. In this paper, FIA, so far formulated only for planar geometry, will be applied for characterizing AUT from near-field cylindrical phaseless measurement. Both the planar and the cylindrical surfaces exhibit computational efficiencies since all numerical integrations can be performed with the fast Fourier transform (FFT) algorithm. The main difference in these cases is that the fields are expanded in cylindrical wave expansions rather than the plane wave spectrum expansion. In this case near-field transformations adopting cylindrical wave expansions use higher order Hankel functions in their formulation which are known to become singular in case of measurements close to the AUT. In the paper we will analyze properties of Hankel function used for forward and backward transformation to make recommendations for cylindrical near-field measurement. Since FIA represents local approach we supplement it with global optimization (GO) [12] to make the algorithm more robust.

The paper is organized in the following manner. The algorithm is described in section 2. The numerical analysis of Hankel functions are in section 3. The applicability and accuracy of the proposed phase retrieval algorithms is illustrated in section 3. The conclusions are reported in section 4.

2. Cylindrical Phase Retrieval Method

FIA as phase retrieval method in antenna measurement was proposed firstly in [10]. In this method only-amplitude measurements were performed over two separated planes in the near-field region of AUT. The scanning planar system could be in any format, such as rectangular, plane-polar, bi-polar, etc. But then for non-rectangular

planar grid formats, the measurement data has to be transformed onto the rectangular grids [10]. The flow chart of FIA is reported under Fig. 2.

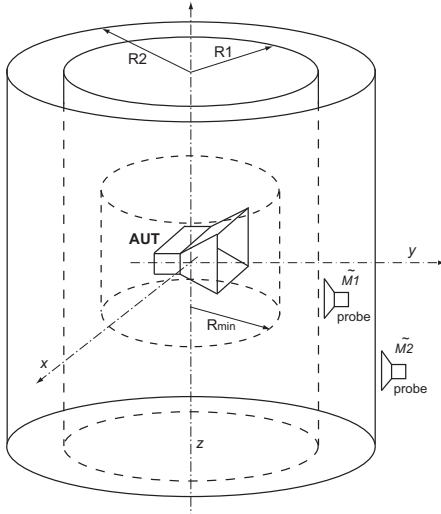


Fig. 1. The principle of the NF antenna phaseless cylindrical measurement.

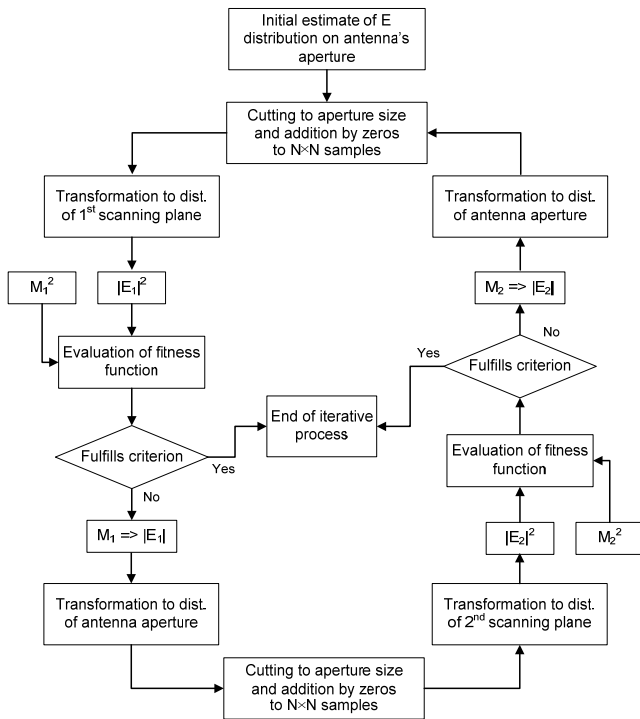


Fig. 2. The flow chart of the Fourier iterative algorithm.

First, an initial guess for the electric field distribution on AUT aperture plane is performed. This initial guess is then propagated to the first plane using the plane-wave spectrum technique. There, an error metric is computed between the evaluated and measured amplitude, as reported in [10]. If the desired error metric is achieved the algorithm is ended. Otherwise, the calculated phase distribution is retained while the amplitude distribution is replaced by the measured amplitude data. The resulted electric field is propagated back to the aperture plane and aperture con-

strain is applied. Now we have a more accurate estimate of the electric field distribution on the antenna aperture. The same procedure is repeated for the second plane. The process of the propagation between these two planes is subsequently performed and the refinement of solution is iteratively made until the defined stopping criterion is reached.

Only several modifications in planar FIA are needed for cylindrical case. Unlike the planar algorithm we have to find the electric field distribution on the cylinder with minimum radius R_{\min} representing antenna aperture, see Fig. 1. Nevertheless, mathematical approach is much complicated. The cylindrical near-field transformations adopting cylindrical vector wave expansions use higher order Hankel functions which limit near-field transformations close to AUT [13]. The numerical analysis of Hankel functions are performed in section 3.

The near-field transformations between two separate cylinders are related by the formulas based on Hankel functions of the first and second kind. The corresponding cylindrical near-fields at R_1 and R_2 of the tangential component electric field $E_z(R_{\min}, \phi, z)$ can be written as

$$E_z(R_i, \phi, z) = \int_{-\pi}^{+\pi} \int_{-\infty}^{+\infty} \left\{ \frac{1}{4\pi^2} \int_{-\pi}^{+\pi} \int_{-\infty}^{+\infty} E_z(R_{\min}, \phi, z) \cdot e^{-jn\phi} e^{jhz} d\phi dz \right\} \times \frac{H_n^{(2)}(\chi R_i)}{H_n^{(2)}(\chi R_{\min})} \cdot e^{jn\phi} e^{-jhz} d\phi dz \quad (i=1,2) \quad (1)$$

and for the tangential component $E_\phi(R_{\min}, \phi, z)$

$$E_\phi(R_i, \phi, z) = \int_{-\pi}^{+\pi} \int_{-\infty}^{+\infty} \left\{ \frac{1}{4\pi^2} \int_{-\pi}^{+\pi} \int_{-\infty}^{+\infty} E_z(R_{\min}, \phi, z) \cdot e^{-jn\phi} e^{jhz} d\phi dz \right\} \times \frac{nh}{\chi^2} \cdot \left[-\frac{1}{R_{\min}} \frac{H_n^{(2)}(\chi R_i)}{H_n^{(2)}(\chi R_{\min})} + \frac{1}{R_i} \frac{H_n^{(2)}(\chi R_i)}{H_n^{(2)}(\chi R_{\min})} \right] \cdot e^{jn\phi} e^{-jhz} d\phi dz + \int_{-\pi}^{+\pi} \int_{-\infty}^{+\infty} \left\{ \frac{1}{4\pi^2} \int_{-\pi}^{+\pi} \int_{-\infty}^{+\infty} E_\phi(R_{\min}, \phi, z) \cdot e^{-jn\phi} e^{jhz} d\phi dz \right\} \times \frac{H_n^{(2)}(\chi R_i)}{H_n^{(2)}(\chi R_{\min})} \cdot e^{jn\phi} e^{-jhz} d\phi dz \quad (i=1,2) \quad (2)$$

where $H_n(\cdot)$ is the Hankel function of order n , $H_n'(\chi R_i) = \partial H_n(\chi R_i) / \partial R_i$, $k = 2\pi/\lambda$, $\chi = \sqrt{k^2 - h^2}$, $h = k \cdot \cos \theta$ and R_i is the radius of the scanning cylinder.

Formulas for inside transformations, from cylinder of radius R_i to the cylinder of radius R_{\min} , have the same form just instead of Hankel functions of the second kind the first kind Hankel functions are applied. Moreover, derived electric field distribution on the scanning cylinder R_{\min} has to be multiplied by the ratio of the scanning cylinders radii (R_i/R_{\min}).

As we mentioned FIA represents a local approach. So a success of FIA as well as other local methods depends on the choice of the initial estimate since the minimized functional suffers with the presence of local minima. We

exploit global optimization techniques to find a suitable estimate in global minimum [12].

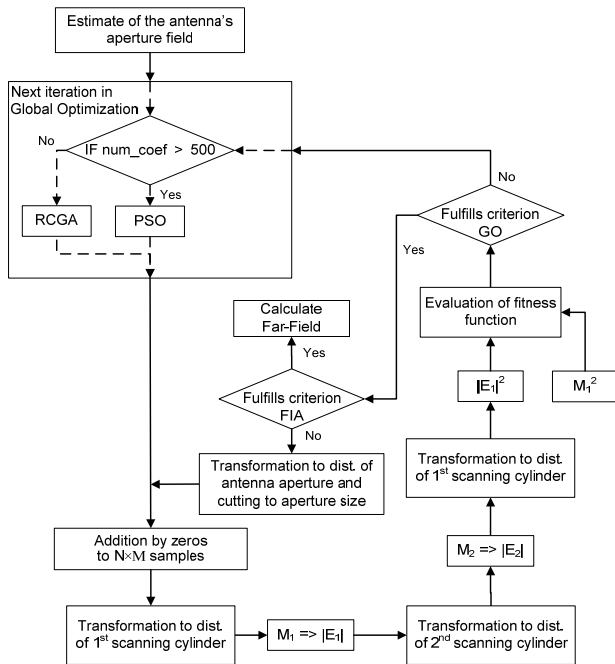


Fig. 3. The flow chart of the hybrid algorithm exploiting a global optimization.

The flow chart of the hybrid algorithm is shown in Fig. 3. We use Real Coded Genetic Algorithm (RCGA) and Particle Swarm Optimization (PSO) as the global optimization tool. Selection of the method depends on the number of optimized variables [12]. The algorithm has two loops, inner loop and outer one. The outer one represents optimization process for finding the initial guess. When the defined criterion of GO is met the process is subsequently switched to inner loop and the initial guess is iteratively refined until the defined stopping criterion of FIA is reached.

The goal of the algorithm is to find such distribution of the electric field intensity on the antenna aperture $E_{z(\phi)}(R_{min}, \phi, z)$ corresponding to the amplitude distributions on scanning cylinders. The proper distribution of the electric field on antenna aperture corresponds to the global minimum of the pre-selected functional [14]

$$F = \sum_{i=1}^N \sum_{j=1}^N \left[|E_1(i, j)|^2 - \tilde{M}_1(i, j)^2 \right]^2 \cdot \tilde{M}_1(i, j). \quad (3)$$

In (3), $E_1(i, j)$ is the computed complex intensity on the first scanning cylinder, and $\tilde{M}_1(i, j)$ is the measured amplitude on the first scanning cylinder. Once the electric field distribution is accurately retrieved, the far-field radiation pattern can be calculated via a standard NF-FF transformation [15].

Thanks to application of global optimization technique, the algorithm does not require any initial guess in the region of the global minima or any additional informa-

tion about AUT. FIA ensures the accuracy comparable with other published methods [5]-[7].

3. Limitation of the NF-NF Transformations

As was mentioned the high order Hankel functions are exploited for transformation between two separate cylinders. We use Hankel functions of the first and second kind depending on if we want to perform forward or backward projection. The numerical analysis of Hankel functions will be done only for tangential component electric field E_z . However, given recommendations will be also valid for component E_ϕ .

Further, we will explain the meaning of variables in transformation formulas since it was not explained correctly yet in opened literature. The formula (1) between two corresponding near-field tangential components of electric field E_z can be simplified into the form

$$E_z(R_2, \phi, z) = F^{-1} \left\{ F[E_z(R_1, \phi, z)] \cdot \frac{H_n^{(2)}(\chi R_2)}{H_n^{(2)}(\chi R_1)} \right\} \quad (4)$$

where F and F^{-1} are Fourier and inverse Fourier transform, respectively. Obviously, the result of transformation depends on order of Hankel function n and argument of Hankel function χR_i .

The order n of Hankel function is limited to $n = -N, \dots, 0, \dots, N$, where $N = kR\xi$, R is the minimum radius which completely encloses the AUT and ξ is a factor slightly larger than one. The order of Hankel function influences electric field distribution in horizontal plane only.

The argument of Hankel function is also function of AUT dimension. The maximum and minimum radii of the cylinders, which are transformed in near field, must satisfy the requirement that

$$kR_{max} > \frac{2kR_{AUT}^2}{\lambda}, \quad (5)$$

$$kR_{min} > kR_{AUT} + kR_{PROBE} + 10 \quad (6)$$

where R_{PROBE} and R_{AUT} are the radii of the test antenna and probe minimum cylinders, respectively. Formula (5) is classic formula defined the border between near-field and far-field of AUT. Formula (6) for the minimum radius of the cylinder was taken from [16] where minimum radius measured sphere has to comply with this requirement. Formula (6) will be subject of further discussion.

There is not only the radius of transformed cylinder in the argument of Hankel function, but also the variable χ . After small modifications the formula for χ can be expressed as

$$\chi = \sqrt{k^2 - h^2} = k \cdot \sin \left(\frac{\pi}{2} - \arctan \left(\frac{H}{2R_{min}} \right) \right) \quad (7)$$

where k is wave number, R_{\min} and H are radius and height of cylinder, respectively. The electric field transformations are performed in forward direction from this surface and backward direction to the surface of this cylinder (see Fig. 4). Obviously, the variable χ depends on ratio H/R_{\min} . This ratio influences electric field distribution in both horizontal and vertical plane. Since the height of cylinder is given the only unknown is the radius R_{\min} . Further, we will examine the influence of R_{\min} on NF-NF transformations.

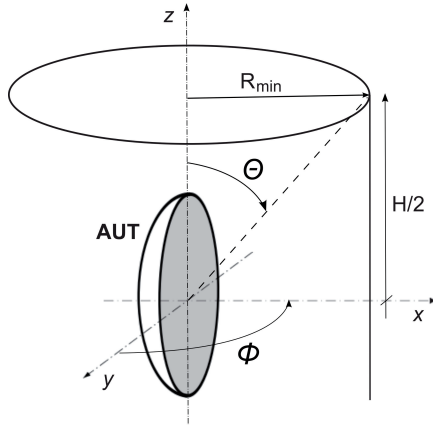


Fig. 4. Geometry of problem.

We investigated the limitation of forward and backward transformations on collinear array consisting of eight z directed elementary dipoles placed along the z axis and $\lambda/2$ equispaced. The array was fed uniformly. The electric field component along z -axis was synthesized from 1λ to the end of NF region (30λ) on cylinders of height $H = 30\lambda$. The minimum radius of cylinder R_{\min} , from which transformations should be performed, is 5.7λ according to (6). It has been assumed that the order of Hankel function is $N = 3$.

The forward transformations were investigated in terms of different ratios ratio H/R_{\min} in Fig. 5 – Fig. 8. The theoretical values of the electric field component E_z in vertical cut ($\phi = 90^\circ$) were confronted with computed electric field distribution obtained by forward transformations from different distances.

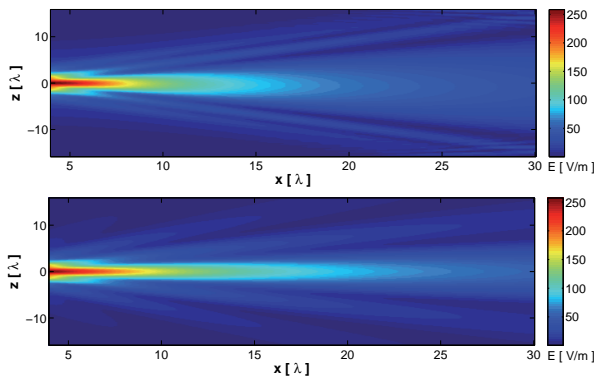


Fig. 5. Comparison of theoretical amplitude distribution of E_z and calculated one obtained by forward transformation; $H/R_{\min} = 7.5$; top: calculated; bottom: theoretical.

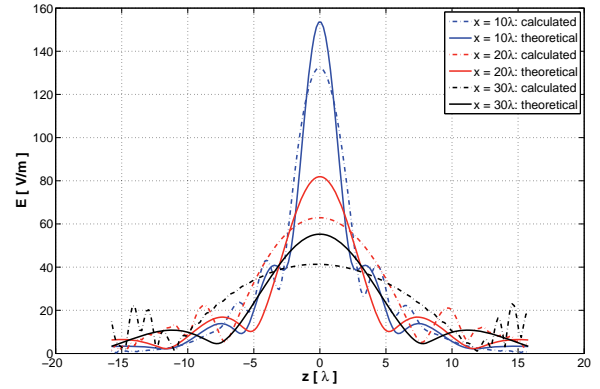


Fig. 6. Comparison of theoretical amplitude cuts of E_z and calculated one obtained by forward transformation; $H/R_{\min} = 7.5$.

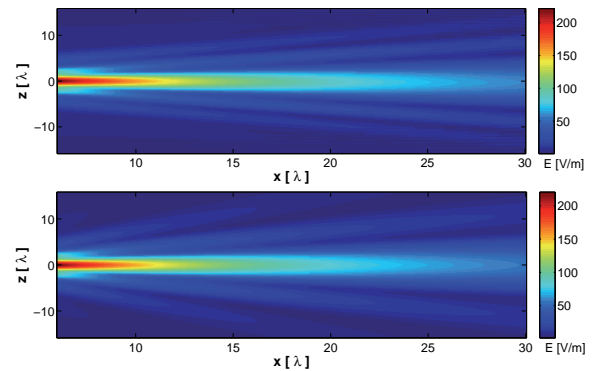


Fig. 7. Comparison of simulated amplitude distribution of E_z and calculated one obtained by forward transformation; $H/R_{\min} = 5$; top: calculated, bottom: theoretical.

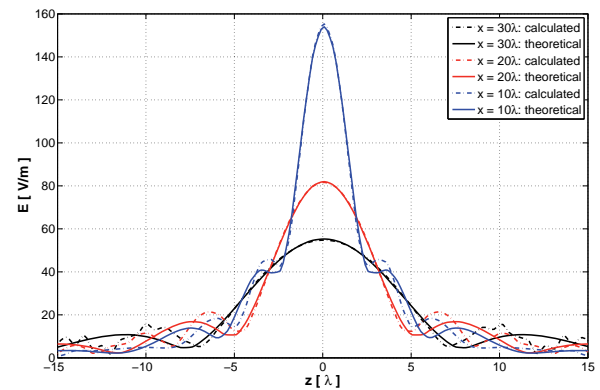


Fig. 8. Comparison of simulated amplitude cuts of E_z and calculated one obtained by forward transformation; $H/R_{\min} = 5$.

Obviously from figures, the calculated near-field distributions are different from the theoretical ones if the ratio H/R_{\min} is larger than 5.5, see Fig. 5 and Fig. 6. If the minimum radius was chosen equal to or larger than the minimum radius $R_{\min} = 5.7\lambda$ ($H/R_{\min} \leq 5.3$) the results were correct. It follows that the minimum radius value R_{\min} , where we are looking for the electric field distribution on antenna aperture, can be chosen according to (6).

Now let us pay attention to the backward transformation. Transformations were made from 30λ , 15λ and 10λ to

the distance of $R_{min} = 6\lambda$. Comparisons of the computed and theoretical electric field distribution in vertical cuts ($\phi = 90^\circ$) are depicted in Fig. 9 – Fig. 13.

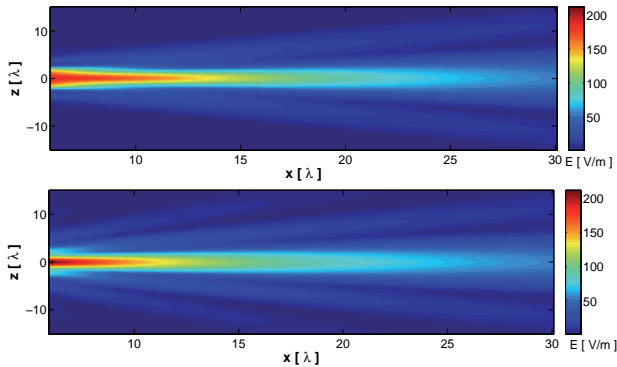


Fig. 9. Comparison of simulated amplitude distribution of E_z and calculated one obtained by backward transformation from the distance 30λ to 6λ ; $H/R_{min} = 5$; top: calculated; bottom: theoretical.

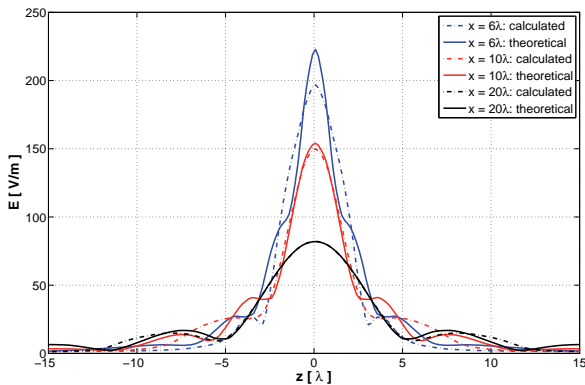


Fig. 10. Comparison of simulated amplitude cuts of E_z and calculated one obtained by backward transformation from the distance 30λ to 6λ ; $H/R_{min} = 5$.

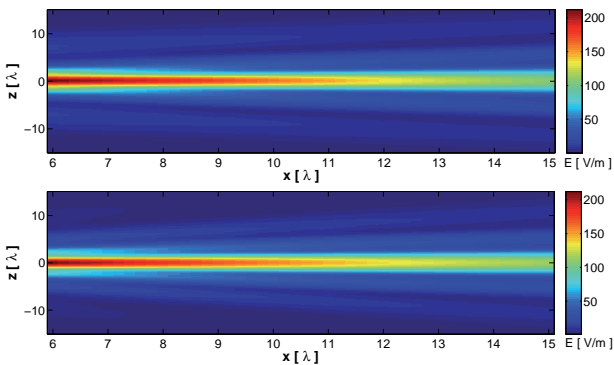


Fig. 11. Comparison of simulated amplitude distribution of E_z and calculated one obtained by backward transformation from the distance 15λ to 6λ ; $H/R_{min} = 5$; top: calculated; bottom: theoretical.

Obviously, the back transformations work well for given ration $H/R_{min} = 5$ and retain the character of the electric field distribution for transformed distance up to 15λ . In opposite case (transformed distance is larger than 15λ), the computed results are slightly different from the theoretical one, see Fig. 9 and Fig.10. It is more evident with increas-

ing backward transformed distance. Therefore, for the backward transformation it is preferable to have distance between cylinders, for which the transformation is carried out, as small as possible.

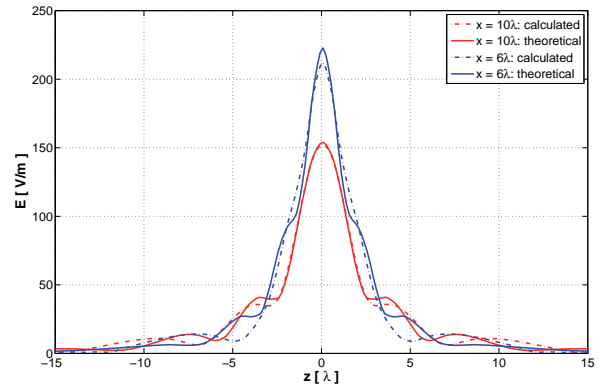


Fig. 12. Comparison of simulated amplitude cuts of E_z and calculated one obtained by backward transformation from the distance 15λ to 6λ ; $H/R_{min} = 5$.

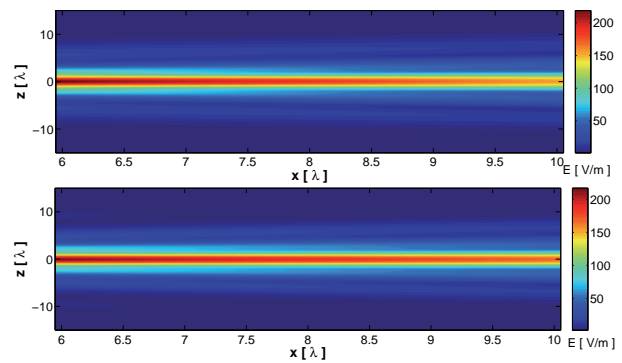


Fig. 13. Comparison of simulated amplitude distribution of E_z and calculated one obtained by backward transformation from the distance 10λ to 6λ ; $H/R_{min} = 5$; top: calculated; bottom: theoretical.

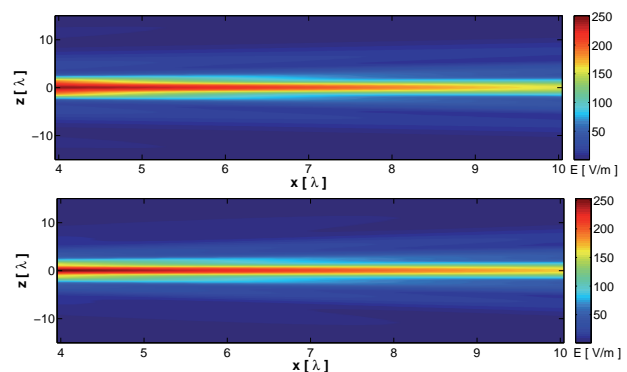


Fig. 14. Comparison of simulated amplitude distribution of E_z and calculated one obtained by backward transformation from the distance 10λ to 4λ ; $H/R_{min} = 7.5$; top: calculated; bottom: theoretical.

In order to verify the formula (6) also for backward transformation we performed the near-field transformation from the distance 10λ to 4λ ($H/R_{min} = 7.5$). Transformed distance is small so the results should be accurate as in the case of transformation from the distance 10λ to 6λ

($H/R_{\min} = 5$); see Fig. 13 and Fig. 15. However, the results are noticeably different; see Fig. 14 and Fig. 15. Even in this case adopting the formula (6) for cylindrical geometry was confirmed as useful.

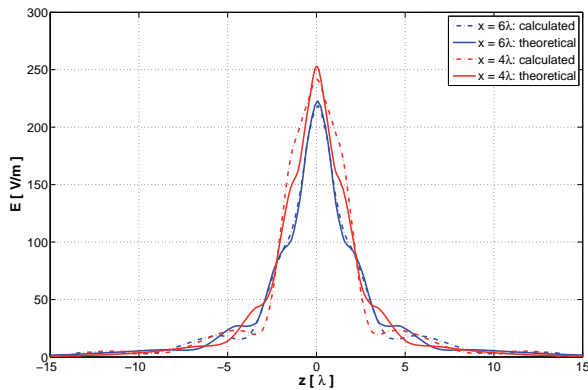


Fig. 15. Comparison of simulated E_z and calculated one obtained by backward transformation from the distance 10λ to 6λ ($H/R_{\min}=5$, blue lines) and to 4λ ($H/R_{\min}=7.5$, red lines).

As we mentioned, the distance between cylinders is important especially for accuracy of backward transformations. So another important task is a proper choice of separation between the scanning cylinders. A high cylinder separation is preferable in order to gain further field information on the second cylinder with the increasing measurement distance. On the other hand, the errors of back transformation are larger with the increasing distance between cylinders.

For the low gain antennas we can adopt recommendation from sphere settings [17] where minimum sphere separation should be at least two wavelengths. In the case of high gain antennas the separation between cylinders could be lower. Respecting performed NF-NF analysis the separation condition could be met with a large margin.

On conclude to the near-field transformations, AUT aperture should be placed as close to the minimum distance according to (6) from the rotation axis to obtain the correct forward NF-NF transformation, see Fig. 16. In addition for the backward NF-NF transformation it is preferable to have a distance between cylinders, for which the transformation is performed, as small as possible with respecting above mentioned comments to separation of scanning cylinders.

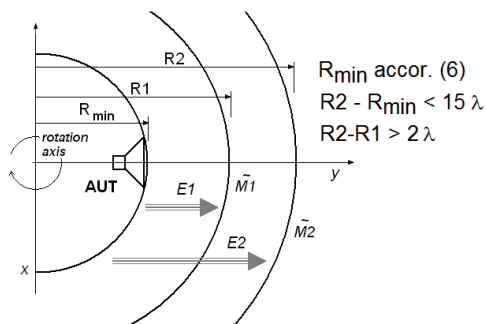


Fig. 16. Recommendations for NF-NF transformations in cylindrical geometry.

4. Experimental Results

The application of the described method was carried out on the radiation pattern reconstruction of horn antenna and dish antenna. The experimental measurements were carried out in collaboration with the Microwave Laboratory of the University of Calabria, Italy [5].

The horn antenna

The rectangular horn antenna had the aperture of the size 70×50 mm. The antenna was analyzed at the frequency 10 GHz. A rectangular waveguide R100 was used as the scanning probe. So, minimum radius R_{\min} is $\sim 4.8\lambda$ according to (6). The order of Hankel function $N = 44$ has been assumed since the length of the horn is 190 mm. The values of the electric field intensity were scanned with the sampling steps $\Delta z = 15$ mm ($\lambda/2$) and $\Delta \phi = 4^\circ$ at two scanning cylinders placed in the distance of 200 mm (6.66λ) and 300 mm (10λ) from the AUT aperture. The height of the cylinders was 690 mm, therefore the valid angle in vertical cut was $\theta_r = \pm 49^\circ$. Aperture field reconstruction was performed on the cylinder of radius $R_{AP} = 190$ mm (6.33λ) (the distance between the AUT aperture and rotation axis).

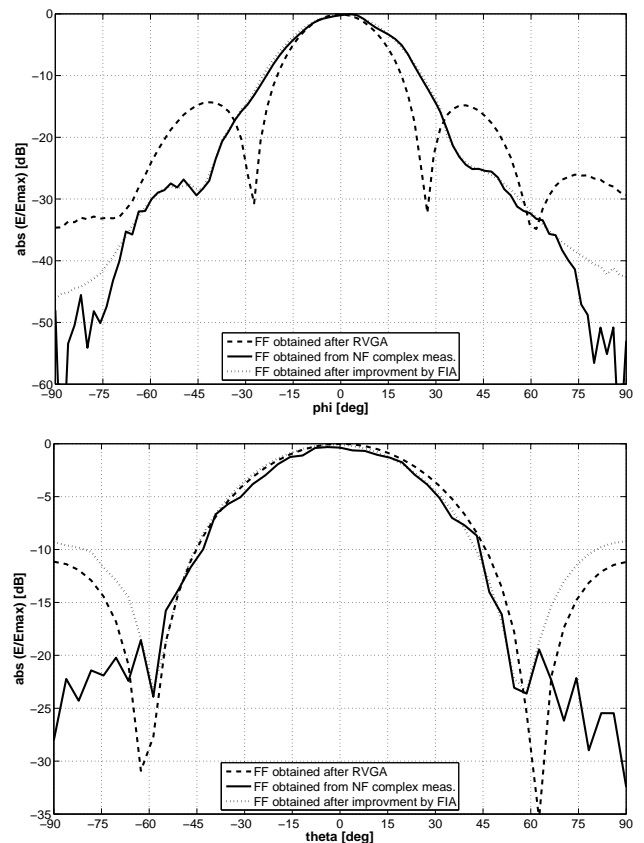


Fig. 17. Reconstructed radiation patterns of the horn antenna after applying the algorithm; top: H plane; bottom: E plane.

The reconstruction was carried out for main electric field component E_z only in domain $\pm 90^\circ$. The aperture field of the antenna contains 20 complex parameters. The results

obtained after 50 iterations using global optimization (RCGA stagnates) are depicted by dashed line in Fig. 17. The accuracy of the reconstructed far-field radiation patterns is not sufficient yet and the algorithm has to continue with inner loop realized by iterative process. The far-field results obtained after using the FIA are depicted by dotted line in Fig. 17. The reconstructed radiation patterns are in good agreement with the pattern gained by the direct transformation in domain of the main lobe i.e. in E plane it is $\pm 55^\circ$ and in H plane it is $\pm 60^\circ$.

The dish antenna

The algorithm was also experimentally tested on a standard X-band dish antenna having a reflector diameter of 0.34 m. A rectangular waveguide R100 was used as the scanning probe. Near-field amplitudes were measured on two cylindrical surfaces placed in distance $R_1 = 200$ mm (6.66λ) and $R_2 = 400$ mm (13.33λ) from AUT aperture. The height of the cylinders was 990 mm, therefore the valid angle in vertical cut was $\theta_v = \pm 48^\circ$. The antenna was analyzed at frequency 10 GHz within a cylindrical grid of 67×145 points along z and ϕ , respectively. Sampling steps $\Delta z = 15$ mm ($\lambda/2$) and $\Delta\phi = 2.5^\circ$ were used. The minimum radius of cylinder R_{\min} , from which the transformations are performed, should be larger than 13.8λ . The order of Hankel function is $N = 72$. The aperture of the antenna is 340 mm \times 340 mm (23 times 23 sampling points). The solu-

sion space contains 529 complex parameters the optimal values of which are to be found out.

The reconstruction was carried out for main electric field component E_z on the cylinder of radius 400 mm ($R_{AP} = 13.33\lambda$). For the initial reconstruction of radiation patterns, we exploited one hundred iterations of PSO. The results are depicted by dashed line in Fig. 18. After that, the algorithm switched into the iterative process. The improved initial estimate is depicted by dotted line in Fig. 18. The agreement between the retrieved far-field and far-field obtained by transformation of the complex near-field data is excellent in domain of main lobe. We can observe that the retrieved far-field becomes less accurate approximately below -30 dB.

5. Conclusions

A phaseless cylindrical near-field transformation algorithm has been presented. The algorithm determines the far-field pattern of an antenna from two amplitude only measurements on cylinders of different radii. The algorithm combines global optimization techniques and Fourier iterative algorithm to avoid the need of any initial guess in the region of the global minima.

The performances of the proposed algorithm have been demonstrated numerically, on synthesized antenna array, as well as on experimental data of the horn antenna and the dish antenna.

Due to the cylindrical measurement configuration, the method exploits cylindrical vector wave expansions using higher order Hankel functions which suffer singularities. In this case, near-field forward and backward transformations have limitations. Therefore we defined some recommendations to the antenna measurement settings presented in the paper.

Acknowledgements

The research leading to these results has received funding from the European Community's Seventh Framework Programme (FP7/2007-2013) under grant agreement no. 230126. The research described in this contribution was performed in the laboratories supported by the SIX project; the registration number CZ.1.05/2.1.00/03.0072, the operational program Research and Development for Innovation.

References

- [1] HELICAR, A. D., HANHAM, S. M., HISLOP, G., DU, J. Terahertz imaging with antenna coupled detectors. In *Proc. of the 3rd European Conference on Antennas and Propagation (EuCAP'09)*. Berlin (Germany), 23-27 March 2009.

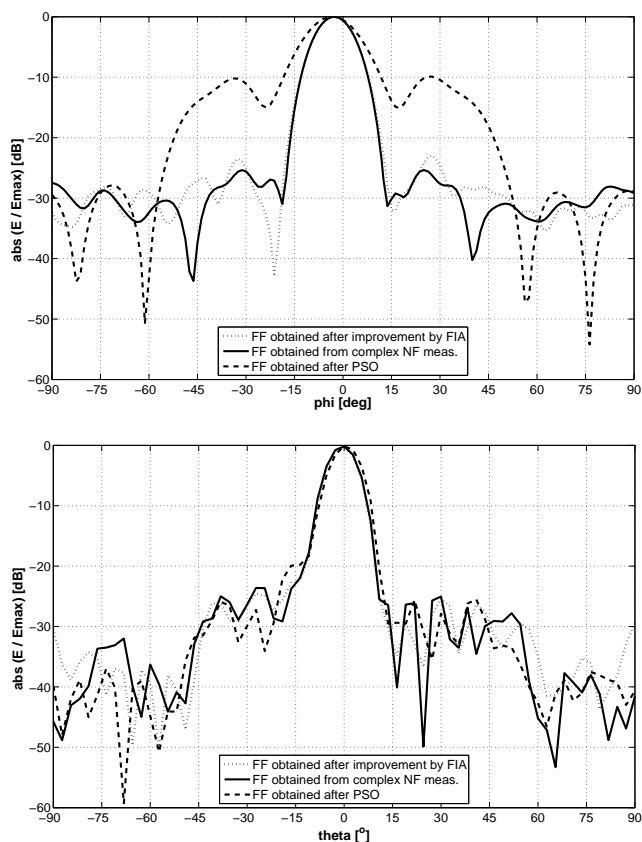


Fig. 18. Reconstructed radiation patterns of the dish antenna after applying the algorithm; top: H plane; bottom: E plane.

- [2] RÄISÄNEN, A. V. et al. Measurement of high-gain antennas at mm- and submm-wavelengths: Challenges and solutions. In *Proc. of the 1st AMTA Europe Symp.* Munich (Germany), 2006, p. 12–17.
- [3] YACCARINO, R. G., RAHMAT-SAMII, Y. Microwave antenna imaging, diagnostics, and phaseless reconstructions. *Int. J. Imaging Syst. Tech.*, 1997, vol. 8, no. 4, p. 396 – 406.
- [4] SCHEJBAL, V., KOVARIK, V., CERMAK, D. Synthesized reference-wave holography for determining antenna radiation characteristics. *IEEE Antennas and Propagation Magazine*, 2008, vol. 50, no. 5, p. 71 - 83.
- [5] COSTANZO, S., DI MASSA, G., MIGLIORE, M. D. A novel hybrid approach for far-field characterization from near-field amplitude-only measurements on arbitrary scanning surfaces. *IEEE Transactions on Antennas and Propagation*, June 2005, vol. 53, no. 6, p. 1866 - 1874.
- [6] ISERNIA, T., LEONE, G., PIERRI, R. A new approach to antenna testing from near field phaseless data: the cylindrical scanning. *IEEE Proc. H*, 1992, vol. 139, p. 363-368
- [7] LAS-HERAS, F., SARKAR, T.-K. A direct optimization approach for source reconstruction and NF-FF transformation using amplitude-only data. *IEEE Transactions on Antennas and Propagation*, April 2002, vol. 50, no. 4, p. 500 - 510.
- [8] FIENUP, J. R. Phase retrieval algorithms: a comparison. *Appl. Opt.*, 1982, vol. 21, p. 2758–2769.
- [9] ANDERSON, A. P., SALI, S. New possibilities for phaseless microwave diagnostics – Part I: Error reduction techniques. *Proc. Inst. Elect. Eng.*, 1985, vol. 132, p. 291-298.
- [10] YACCARINO, R. G., RAHMAT-SAMII, Y. Phaseless Bi-Polar planar near-field measurements and diagnostics of array antennas. *IEEE Transactions on Antennas and Propagation*, 1999, vol. 47, no. 3, p. 574 – 583.
- [11] RAZAVI, S. F., RAHMAT-SAMII, Y. A new look at phaseless planar near-field measurements: limitations, simulations, measurements, and a hybrid solution. *IEEE Trans. Antennas Propag.*, 2007, vol. 49, no. 2, p.170-178.
- [12] PUSKELY, J., NOVÁČEK, Z. Application of the global optimization approaches to planar near-field antenna phaseless measurements. *Radioengineering*, 2009, vol. 18, no. 1, p. 9 - 17.
- [13] CHEW, W., JIN, J., MICHIELSEN, E., SONG, J. *Fast and Efficient Algorithms in Computational Electromagnetics*. Artech House, Inc, 2001.
- [14] PUSKELY, J., NOVÁČEK, Z. New look to real valued genetic algorithm used to reconstruct radiation patterns. In *Proceedings of the 15th Conference Radioelektronika 2009*. Bratislava (Slovakia), 2009, p. 299 - 302.
- [15] BUCCI, O.M. GENNARELLI, C. RICCIO, G. Efficient near-field-far-field transformation with cylindrical scanning by a finite and non redundant number of data. In *Antennas and Propagation Society International Symposium*, 1995. AP-S. Digest, vol. 1, June 1995, p. 256 – 259.
- [16] HANSEN, J. E. Spherical near-field antenna measurements. *IEE Electromagnetic Wave Series* 26, Exeter, UK, 1988.
- [17] SCHMIDT, C. H., RAZAVI, S. F., EIBERT, T. F., RAHMAT-SAMII, Y. Phaseless spherical near-field antenna measurements for low and medium gain antennas. *Advances in Radio Science*, 2010, vol. 8, p. 43–48.

About Author...

Jan PUSKELY was born in Přerov, the Czech Republic, in 1982. He received his master's degree in 2007, and Ph.D. degree in 2011, both in Electrical Engineering from Brno University of Technology. At present, he is with the Department of Radio Electronics, Brno University of Technology. His research interest is focused on measurements in the near field of antennas.